Journal of Hydrology 612 (2022) 128023

Contents lists available at ScienceDirect

Journal of Hydrology

journal homepage: www.elsevier.com/locate/jhydrol

Research papers

Elaborate simulation and predication of the tunnel drainage effect on karst groundwater field and discharge based on Visual MODFLOW

Yuxiang Lv [a,b], Jing Jiang [b], Li Chen [b], Wei Hu [c], Yongjun Jiang [a,*]

[a] Chongqing Key Laboratory of Karst Environment & School of Geographical Sciences, Southwest University, Chongqing 400715, China
[b] Hydrogeology & Engineering Team 208, Chongqing Bureau of Geological Exploration (Chongqing Reconnaissance and Design Academy of Geological Disasters Prevention and Treatment Engineering), Chongqing 400700, China
[c] Chongqing Survey and Mapping Institute, Chongqing 401121, China

ARTICLE INFO

This manuscript was handled by Zhang Wen, Editor-in-Chief, with the assistance of Corrado Corradini, Associate Editor

Keywords:
Karst groundwater flow field
Tunnel excavation
Modeling
Karst trough valley

ABSTRACT

The groundwater drawdown caused by tunnel excavation can change the hydrogeological flow system in karst areas. However, how to overcome the heterogeneity in karst aquifers and accurately evaluate the impacts of tunnel excavation on karst groundwater flow field and resources remains largely unknown. In this study, through geophysical prospecting, hydrogeological drilling and test, and observations in 4 years, the depth, scale and spatial distribution of underground river conduits and hydrogeological parameters before and after tunnel excavation are obtained, and the groundwater flow field before and after tunnel excavation was established by Visual MODFLOW. Observation and simulation indicate that two ponds, 5 epikarst springs, 1 borehole, 1 railway tunnel and the underground river system were affected during tunnel excavation. The drainage effect of tunnel is more significant in dry season. Three depression cones are formed, and there is a drawdown of 10 ~ 30 m due to the tunnel excavation. The simulation results predict that the drainage effect is more significant when the tunnels are below the groundwater level in the dry season. Driven by the increase of precipitation and tunnel drainage, the seasonal variation of underground river discharge is exacerbated, and the groundwater level near the tunnel in the rainy season is lower than that in the dry season, which is opposite to that in natural state. The groundwater flow budget calculation and prediction suggest that the net loss of groundwater storage was 6.1×10^5 m^3 during tunnel excavation, and the net loss of groundwater storage is about 1.7×10^5 m^3 one year after the tunnels were completed, and meanwhile the depression cones continue to expand. The increase of precipitation raises the groundwater level and alleviates the drainage effect, but the increased precipitation recharge is less than groundwater discharge and tunnel drainage, so there is still a loss of groundwater storage. It is difficult to restore the groundwater flow field and discharge in a short time. This study provides evidence and a useful method to quantitatively evaluate the effects of tunnel excavation on the groundwater flow field and to inform better measures to protect karst groundwater resources.

1. Introduction

Karst aquifers, as a source of drinking water to almost a quarter of the world's population, are particularly vulnerable to environmental changes and human impacts due to their unique hydrogeological characteristics (Ford and Williams, 2007). Efficient transport relies strongly on road and railway tunnels in karst areas, both for long-distance traffic and in metropolitan areas (Butscher et al., 2011). Tunnels drilled through karst areas often cause many problems (e.g., water inrush, karst collapse and groundwater drawdown). Inflows to tunnels reduce the groundwater level (Kim et al., 2001), expand the groundwater supply boundary (Vincenzi et al., 2009), and thus change the natural hydrogeological flow around the tunnel.

In recent decades, many efforts have focused on developing more sophisticated analytical solutions to estimate the water inflow during tunneling (Goodman et al., 1965; El Tani, 2003; Perrochet, 2005; Kolymbas and Wagner, 2007; Park et al., 2008; El Tani, 2010; Coli and Pinzani, 2014; Maréchal et al., 2014), using more reasonable methods to evaluate the impacts of tunnel excavation on water resources and hydrological processes (Laura, et al., 2003; Vincenzi et al., 2014; Chiu and

* Corresponding author at: Yongjun Jiang, Chongqing Key Laboratory of Karst Environment & School of Geographical Sciences of Southwest University, Chongqing 400715, China.
E-mail address: jiangjyj@swu.edu.cn (Y. Jiang).

https://doi.org/10.1016/j.jhydrol.2022.128023
Received 11 February 2022; Received in revised form 5 May 2022; Accepted 2 June 2022
Available online 11 June 2022

Chia, 2012; Mossmark et al., 2015), trying more accurate models to simulate the groundwater flow around tunnels (Butscher et al., 2011; Butscher, 2012; Koyama et al., 2012; Xia et al., 2018; Hadi and Arash, 2018; Zhang et al., 2019; Scheidler et al., 2019; Li et al., 2020), and using tree ring and isotope methods to track the changes in plant production rates and physiological processes caused by groundwater drawdown (Zheng et al., 2017; Liu et al., 2019; Cao et al., 2020).

Continuous and high-resolution monitoring can reflect the real-time changes in surface water and groundwater due to tunnel excavation. However, because of the heterogeneity of karst groundwater and the inadequate number of boreholes and natural springs near tunnel sites, the groundwater flow field must be partially studied by groundwater simulation software. Hydrological modeling has been used for simulations of underground water flow regimes or seepage fields under the influence of tunnels (Raposo et al., 2010; Chen et al., 2020); for example, Visual MODFLOW, developed by the United States Geological Survey (USGS), is widely used. In this approach, the groundwater flow is described by the continuity and momentum balance equations that are mostly based on Darcy's law (Zheng et al., 2020). Under more complex groundwater flow conditions, non-Darcian flows have also been considered (Chen et al., 2020). Based on the partial differential equation that describes groundwater flow, Visual MODFLOW has become a valuable tool for studying water resources in karst aquifers. Nevertheless, the turbulence and flow in karst conduits have not been considered. In view of the karst water system with the coexistence of conduits, fractures and pores, this model has been optimized and improved (e.g., MODFLOW-CFP) and demonstrated to be effective in recent years (Shoemaker et al., 2008; Hill et al., 2010; Hu et al., 2012; Gallegos et al., 2013; Chang et al., 2015; Giese et al., 2018; Zargham, et al., 2018; Aliouache et al., 2019). However, although MODFLOW-CFP can calculate the flow process of different nodes, it does not consider the hydrodynamic process inside the conduit, and the description of the conduit characteristics is relatively vague. It is assumed that the conduits are relatively uniform aqueous media, and the heterogeneity is ignored in the selection of relevant parameters. Regardless of which model is used, the accuracy of the karst conduit parameters is the key to the effectiveness of the model. Geophysical prospecting technology is an effective means to analyze underground karst. To determine the depth, shape and spatial distribution of underground river conduits, many explorations have been carried out by using magnetotelluric sounding (EH4), the high-density resistivity method, the transient electromagnetic method (TEM), the shallow seismic reflection method, the audio magnetotelluric method (AMT), electrical resistivity tomography (ERT), etc., and the combination of different methods has proven to be effective in different cases (Li et al., 2008; Gan et al., 2010; Mastrocicco, et al., 2010; Parsekian, et al., 2015; Chen, et al., 2018). Hydrogeological drilling can verify the interpretation of geophysical prospecting and directly reflect the characteristics of underground karst. Tracer tests, pumping tests and water pressure tests are common methods used to obtain hydrogeological parameters (Vincenzi et al., 2009; Jiang, et al., 2016; Zheng et al., 2020). Therefore, the location, shape, characteristics and hydrogeological parameters of karst conduits should be found out by the combination of geophysical prospecting, hydrogeological drilling and various hydrogeological tests, and the hydrogeological model established in this way can be more effective.

Studies have shown that tunnel excavation affects karst groundwater resources and flow field (Attanayake and Waterman, 2006; Moon and Jeong, 2011; Lv et al., 2020). First, tunnel drainage destroys the aquifer structure. Then, surface water and groundwater drain, forming a depression cone, which expands with drainage time until the tunnel drainage fully accounts for the recharge from the boundary, and therefore, the groundwater flow field and water resources are changed. However, due to the complexity of karst geological structures and the multidirectional heterogeneity of karst groundwater, the changes of karst groundwater flow field, groundwater resources and hydrological process caused by groundwater drawdown remain largely unknown, and the response of karst hydrogeological systems to tunnel drainage may be more complex than expected. As an open dynamic system, the changes of karst groundwater are highly sensitive to external climatic conditions at seasonal, monthly, daily, or even hourly scales (White, 2007; Liu et al., 2007). Driven by the external environment and human engineering activities, the karst groundwater system may be more sensitive. The change of precipitation may aggravate or alleviate the impact of tunnel excavation on karst groundwater. Therefore, it is necessary to predict and evaluate the response of karst groundwater flow field and discharge to precipitation under the condition of tunnel interference.

Besides, many studies believe that after the completion of the tunnel lining, the tunnel will no longer provide drainage or the drainage will be very small, and the groundwater level and storage will return to the previous state (Gisbert et al., 2009; Zheng et al., 2020). Actually, karst conduits and fissures were exposed in the process of tunnel excavation, and more fissures appeared because of the impact of blasting vibration, so the hydrogeological parameters (such as hydraulic conductivity) in the tunnel site area changed accordingly. Therefore, whether the groundwater resources and groundwater flow field can be restored remains to be clarified.

In this study, based on geophysical prospecting, hydrogeological drilling and tests, and observations in 4 years, the depth, scale and spatial distribution of underground river conduits and hydrogeological parameters before and after tunnel excavation are obtained, and the groundwater flow field before and after tunnel excavation was established by Visual MODFLOW in a karst trough valley in Southwest China. Here the following objects were addressed: to reveal the variation process of tunnel drainage, groundwater level and discharge, through high-resolution observation; to quantitatively evaluate the change of groundwater flow field and the loss of groundwater storage, through simulation and calculation of the groundwater flow budget; to identify the response of groundwater level and discharge to precipitation under tunnel interference, through simulation and predication; to analyze the recovery of groundwater resources through simulation and predication of the groundwater flow budget. This study will provide a better scientific basis for the planning, site selection and construction decision-making associated with tunnels in karst areas.

2. Data and methods

2.1. Study area

The Mingyuexia karst trough valley (106° 48′ 52″~106° 59′ 06″ E, 29° 38′ 52″ ~29° 54′ 47″ N), which has an area of 63.56 km^2, is located in the southern part of the Mingyue Mountains in northeastern Chongqing, Southwest China (Fig. 1). The regional climate is characterized by a humid subtropical monsoon climate with an average annual precipitation of 1100 mm (approximately 65% of precipitation occurs during the rainy season from May to September) and a mean annual air temperature of 18 °C.

The Mingyuexia karst trough valley is located in the Mingyuexia anticline, extends north–south, and consists of a karst valley in the middle and two ridges on both sides. The karst valley, which is composed of carbonate rocks corresponding to the Lower Triassic Daye (T_1d) and Jialingjiang Formations (T_1j) and the Middle Triassic Leikoupo Formation (T_2l) is located at the axis of the anticline, with an elevation of 450 ~ 600 m (Fig. 1); the ridges and slopes, which are composed of clastic rocks corresponding to the Upper Triassic Xujiahe Formation (T_3xj) and Jurassic (J) strata are located on the wings of the anticline, with an elevation range of 350 ~ 700 m. This karst valley is approximately 27 km long and 2 km wide. Due to differential dissolution, three parallel secondary valleys have formed in the eastern, middle and western areas (Fig. 1).

Horizontally, the northern surface watershed (600 ~ 850 m above sea level) is the recharge boundary of the groundwater system in the Mingyuexia karst trough valley, and the underground river in the south

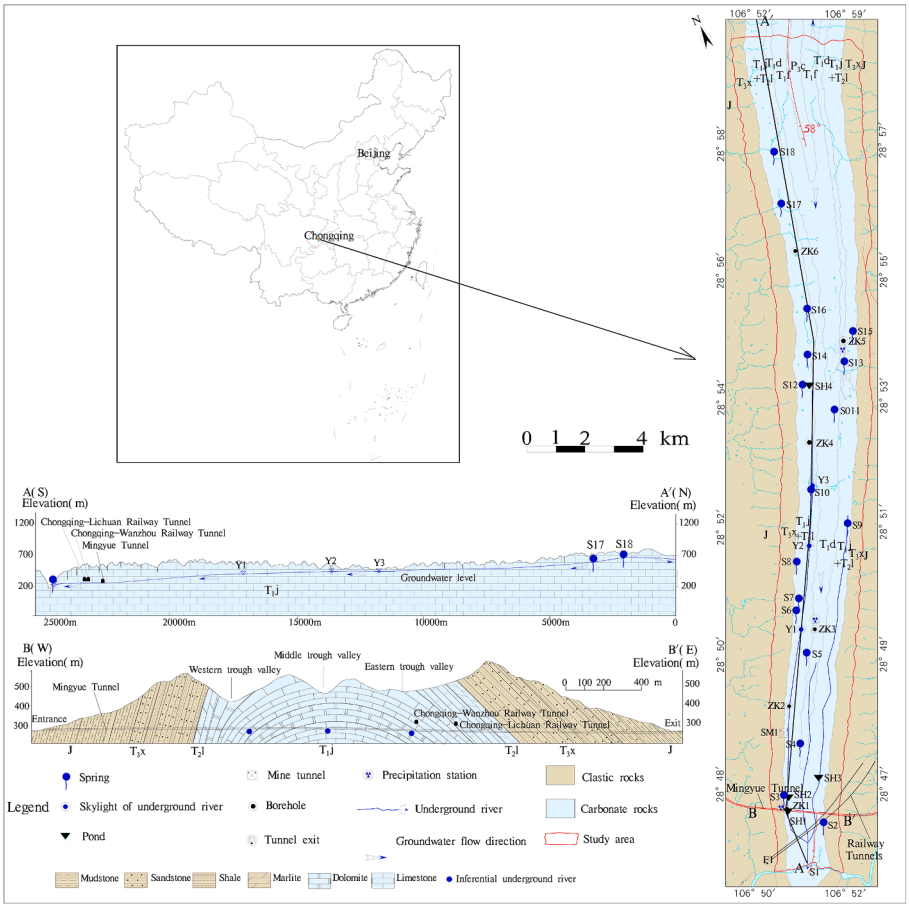

Fig. 1. Hydrogeological map of the Mingyuexia karst trough valley in Chongqing.

is the only outlet of the groundwater system, which discharges into the Yulin River, (180 ~ 200 m above sea level). The sandstone and shale of the Upper Triassic Xujiahe Formation (T_3xj) on the eastern and western sides form the water separation boundary. Vertically, the mudstone of the Lower Triassic Feixianguan Formations (T_1f) is the floor that separates the water, and the limestone, dolomite and argillaceous limestone of the Lower Triassic Daye (T_1d) and Jialingjiang Formations (T_1j) and the Middle Triassic Leikoupo Formation (T_2l) are aquifers with thicknesses of 480 ~ 500 m. Many vertical open fractures in the limestone and dolomite in the valley provide the basic conditions for the formation of karst depressions and sinkholes. Rainwater and surface water quickly enter the karst aquifer through sinkholes, fissures or shafts, and the water then migrates from north to south, and finally discharge in the form of karst springs or underground rivers. Before tunnel excavation, there were 30 epikarst springs (0 ~ 5 L/s) and 1 underground river (45 ~ 1800 L/s) in the karst trough valley. Three karst branch conduits of the underground river are present in the three secondary karst valleys and converge to form a main conduit in the south, which intersects and discharges into the Yulin River, with an outlet elevation of 185 m.

2.2. Tunnel excavation in the Mingyuexia karst trough valley

The Mingyue Mountains are located on the northeastern edge of the Chongqing metropolitan area, and the mountain range is an obstacle to urban expansion and external communication. The construction of tunnels is an inevitable choice for urban development. The Mingyue Tunnels are double track tunnels that are part of the Third Ring Expressway in Chongqing, with lengths of 3220 m and 3270 m, elevations of 260 ~ 290 m, and a maximum depth of 380 m. The tunnels were excavated from both ends toward the middle simultaneously, and construction started in March 2018 and was completed in October 2020. The tunnels pass through mudstone, sandstone and shale of the Jurassic and Upper Triassic Xujiahe Formations and limestone of the Lower Triassic Jialingjiang Formation, with maximum water inflows of 6.25 L/s and 17.36 L/s, respectively (Fig. 2). Two north–south-directed underground river conduits (P1 and P2) were exposed and were 11 ~ 12 m high and 5 m wide in July and September 2019. The underground water flowed into the Mingyue Tunnels from the karst conduit south of P1 after precipitation, with a flow of 11.1 L/s, while the conduit north of P1 and P2 had no water inflow.

Two other parallel railway tunnels in the karst trough valley cross the Mingyue Tunnels in plan view (Fig. 1), but they are vertically 15 ~ 30 m higher. The Chongqing-Wanzhou Railway Tunnel was completed in 2014, and has an elevation of 301 m, which is above the groundwater level. A large number of dry karst caves were encountered during the construction period, without a large amount of flowing water, and there is currently no drainage. The Chongqing-Lichuan Railway Tunnel was completed in 2013 and has an elevation of 301 m, which is above the groundwater level, and the tunnel water inflow measured in December 2017 was 25.397 L/s. Some epikarst springs dried up or were reduced after the excavation of these two tunnels.

2.3. Data acquisition

Hydrogeological surveys, typical geological sections and cave measurements were performed in the hydrogeological unit of the Mingyue Tunnels to determine the karstification, aquifer thickness, water yield, recharge-runoff-discharge conditions, discharge and water level of different water bodies before tunnel excavation.

There are 34 observation stations on the northern and southern sides

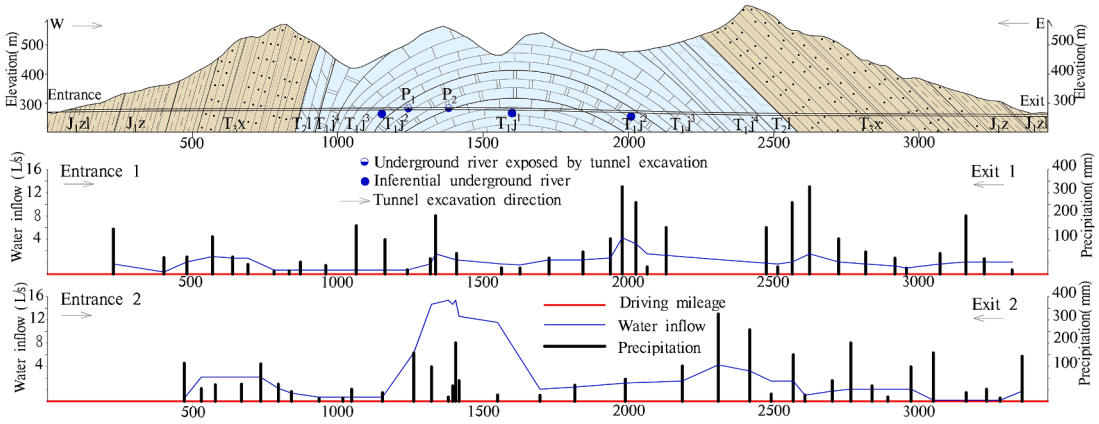

Fig. 2. Geological section of the Mingyue Tunnels and water inflow during tunnel excavation.

of the Mingyue Tunnels, including 4 ponds, 17 springs, 1 underground river and 3 skylights, 1 railway tunnel, 1 manual observation station in a coal mine tunnel, 6 automatic groundwater level observation stations in boreholes and 3 automatic rainfall stations (Fig. 1, Table 1). Moreover, the water inflows at the 4 exits and entrances of the Mingyue Tunnels under construction were observed in real time. These observation stations constitute a monitoring network covering supply, runoff and discharge areas, and the data can reflect the changes in the karst groundwater flow field. The discharge and water level are recorded by a triangular weir, rectangular weir and water level gauge in the manual observation station once every 3 ~ 5 days, with an accuracy of ± 0.5 mm; the rainfall and water level are observed by a water level-precipitation integrated automatic observation station (YT-YT-0100) or a water level automatic observation station (YT-YL-0300) once every half an hour, with an accuracy of ± 0.1 mm. From March 2018 to October 2021, 9500 manually observed discharge and water level data and 42,000 automatically observed water level and rainfall data were obtained.

The precipitation infiltration coefficients (α) of different strata are calculated by measuring the discharge of springs and underground rivers in the dry season; the thickness of different strata is obtained by measuring the stratigraphic profile; the depth, scale and spatial distribution of karst conduits are identified through geophysical exploration and hydrogeological boreholes; and the permeability coefficients (*k*) are obtained by pumping tests and water pressure tests. In 2021, 21 boreholes (SW1-SW21) were drilled in the study area. The hydrogeological parameters and water level after tunnel excavation are mainly from these boreholes.

Table 1
Basic information on the observation stations.

Number	Trough valley	Elevation (m)	Distance and orientation from tunnel (m)	Aquifer	Initial discharge (L/s)	Initial water level (m)	Observation methods
S1	Middle	162	1700 S	T_1j^1	32.548		Rectangular weir
S2	East	575	450 S	T_1j^3	0.008		Volumetric method
S3	West	454	350 N	T_1j^3		453.56	Water level gauge
S4	Middle	498	2100 N	T_1j^1	0.006		Volumetric method
S5	Middle	600	5200 N	T_1j^1		599.34	Water level gauge
S6	West	532	6700 N	T_1j^3	0.25		Volumetric method
S7	West	560	7100 N	T_1j^3		559.76	Water level gauge
S8	West	521	8300 N	T_1j^3		520.79	Water level gauge
S9	East	493	9800 N	T_1j^3		491.37	Water level gauge
S10	West	478	10800 N	T_1j^2	0.042		Volumetric method
S11	East	528	13600 N	T_1d		527.78	Water level gauge
S12	West	505	14400 N	T_1j^2		504.48	Water level gauge
S13	East	538	15000 N	T_1j^1			Water level gauge
S14	West	518	15400 N	T_1j^2	0.089		Triangular weir
S15	East	518	16400 N	T_1j^2	0.018		Triangular weir
S16	West	539	16900 N	T_1j^1	0.093		Triangular weir
S17	West	526	20600 N	T_1j^2	4.955		Rectangular weir
S18	West	533	22400 N	T_1j^2	1.63		Rectangular weir
F1	West	240	1700 S	T_1j	25.397		Rectangular weir
SM1	West	500	2600 N	T_3x	0.2		Volumetric method
Y1	West	496	6100 N	T_1j^2		415.35	Water level gauge
Y2	West	485	9100 N	T_1j^1		440.34	Water level gauge
Y3	West	485	11140 N	T_1j		442.41	Water level gauge
ZK1	West	421	Above the tunnel	T_1j^3		275.46	YT-YT-0100
ZK2	West	470	3600 N	T_1j^3		343.5	YT-YL-0300
ZK3	Middle	520	6100 N	T_1j, T_1d		410	YT-YT-0100
ZK4	West	493	12600 N	T_1j^1		481	YT-YL-0300
ZK5	East	528	16000 N	T_1j^2		493	YT-YT-0100
ZK6	West	547	20000 N	T_1j^1,T_1d		537.55	YT-YL-0300
SH1	West	417	100 S			411.43	Water level gauge
SH2	West	435	360 N			429.46	Water level gauge
SH3	East	481	1100 N			479.7	Water level gauge
SH4	West	503	14500 N			502.34	Water level gauge

2.4. Modeling

2.4.1. Conceptual model and boundary conditions

Visual MODFLOW was developed by Waterloo Hydraulic Inc. in Canada and is based on MODFLOW software (1984) of the USGS. In this paper, we use Visual MODFLOW to simulate three-dimensional saturated flow. The karst aquifers of the Lower Triassic Jialingjiang Formation (T_1j), Lower Triassic Daye Formation (T_1d) and Middle Leikoupo Formation (T_2l) are the main target layers of the simulation, and they can be generalized into heterogeneous anisotropic phreatic confined water aquifers with unified groundwater levels. The permeability of groundwater in the Jurassic (J) strata, Upper Triassic Xujiahe Formation (T_3xj) and Feixianguan Formations (T_1f) is poor, so these strata are treated as aquicludes.

Horizontally, according to the groundwater level monitoring results, the maximum impact range of the tunnel is 7.1 km in the north, so the surface watershed, which is 8 km from the Mingyue Tunnels, is taken as the northern boundary of the simulation area (the first-kind boundary Γ_1). The outlet of the underground river (S_1) is the discharge boundary in the south (the second-kind boundary Γ_2). Some springs in the study area drained due to the construction of the two railway tunnels before 2013. At present, the flow of surface karst springs in the study area is mostly less than 0.1L/s (Table 1), accounting for a very small ratio of the underground river outlet flow (45 ~ 1800 L/s). Therefore, the underground river outlet is taken as the only outlet of this groundwater system in this study. There is no hydraulic connection between the pond and groundwater, so the pond is not used as a source or sink item during modeling. The Upper Triassic Xujiahe Formation (T_3xj) on the eastern and western sides is treated as impervious boundaries, and the simulated area is 17.38 km^2. Vertically, the Feixianguan Formation (T_1f) is an aquiclude, and it is also the bottom boundary of the shallow groundwater system. The average elevation of the top of the Feixianguan Formation (T_1f) in the simulation area is approximately 0 m (burial depth of 450 ~ 800 m). Therefore, the elevation of 0 above sea level is taken as the bottom boundary of the hydrogeological model. The hydrogeological system is recharged by precipitation. The surface topography as interpolated with a 30 m × 30 m horizontal resolution is taken as the top boundary. The hydrogeological map of the simulation area is shown in Fig. 3.

2.4.2. Mathematical model

Groundwater flow is generalized into heterogeneous isotropic and unstable groundwater flow systems. The corresponding mathematical model is established as follows:

$$\begin{cases} \dfrac{\partial}{\partial x}\left(k_x\dfrac{\partial h}{\partial x}\right)+\dfrac{\partial}{\partial y}\left(k_y\dfrac{\partial h}{\partial y}\right)+\dfrac{\partial}{\partial z}\left(k_z\dfrac{\partial h}{\partial z}\right)+W=u_s\dfrac{\partial h}{\partial t} \\ h(x,y,t)|_{t=0}=h_0(x,y) \qquad (x,y)\in D \\ h(x,y,z,t)|\Gamma_1=h(x,y,z,t) \qquad (x,y,z)\in\Gamma_{1,t}\geqslant 0 \\ k\dfrac{\partial h}{\partial n}\Big|\Gamma_2=q(x,y,z,t) \qquad (x,y,z)\in\Gamma_{2,t}>0 \end{cases} \tag{1}$$

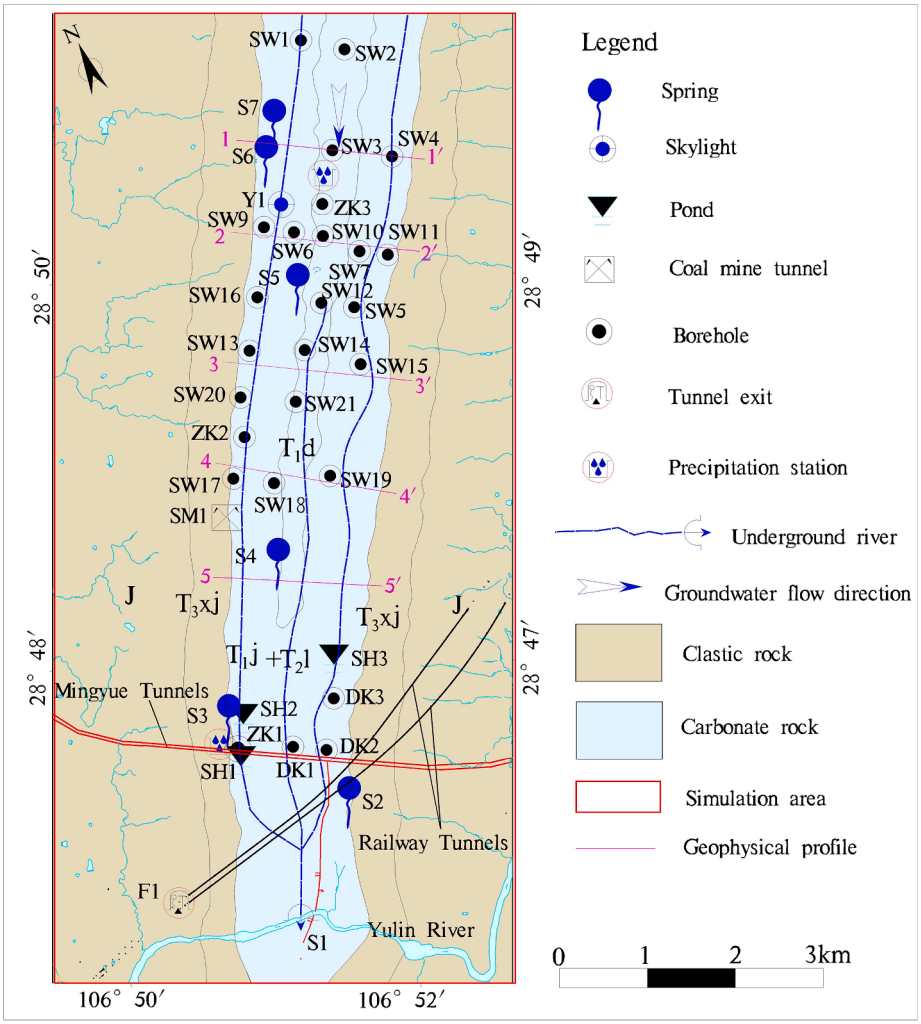

Fig. 3. Hydrogeological boundary, boreholes and geophysical profile in the simulation area.

where k_x, k_y, and k_z are the values of the permeability coefficients in the X, Y and Z directions, respectively; h is the groundwater level; W is the discharge per unit volume; u_s is the specific storage; t is the time; D is the simulation area; Γ_1 is the boundary with a fixed water head; Γ_2 is the boundary with a fixed water flow; n is the outer normal direction on the boundary; and q is the discharge.

2.4.3. Geological and hydrogeological parameters

Eight geological profiles were measured in the simulation area (Fig. 3). The thickness of the Daye Formation (T_1d) is 161 ~ 221 m; the thickness of the Jialingjiang Formation (T_1j) is 397 ~ 419 m; the thickness of the Leikoupo Formation (T_2l) is 19 ~ 113 m; the thickness of the Xujiahe Formation (T_3xj) is 372 ~ 419 m; the thickness of the Ziliujing Formation (including the Zhenzhuchong Formation) (J_1z) is 377 ~ 404.4 m; and the thickness of the Xintiangou Formation (J_2x) is between 111 ~ 118 m.

The precipitation was obtained from 10 springs, and the precipitation infiltration coefficient was calculated (Formula 2) from discharge measurements in the dry season before tunnel excavation (December 2017) and after tunnel excavation (December 2020). Before and after tunnel excavation, the precipitation infiltration coefficient of the Jurassic stratum (J) is 0.03; the precipitation infiltration coefficient of the sandstone section in the Xujiahe Formation (T_3xj^2, T_3xj^4, T_3xj^6) is 0.18 and 0.2 respectively, the precipitation infiltration coefficient of the mudstone section in the Xujiahe Formation (T_3xj^1, T_3xj^3, T_3xj^5) is 0.03, and the precipitation infiltration coefficient of the Leikoupo Formation (T_2l) is 0.35 and 0.4; and the precipitation infiltration coefficients of the Jialingjiang Formation (T_1j) are 0.48 and 0.50, respectively.

$$\alpha_i = \frac{3.15Q_i}{0.1H \cdot F_i} \tag{2}$$

where α_i is the precipitation infiltration coefficient; Q_i is the spring discharge in the dry season (L/s); F_i is the drainage area of spring (km^2); and H is the annual precipitation (mm).

The permeability coefficient (k) is obtained from the pumping tests and water pressure tests performed in the 26 boreholes (Table 2). Based on the permeability coefficients of boreholes ZK1 ~ ZK3 and boreholes DK1 ~ DK3, the initial value of the permeability coefficient in the simulation area is determined via interpolation before the excavation of the Mingyue Tunnels; based on the permeability coefficients of boreholes SW1 ~ SW21, the initial value of the permeability coefficient in the simulation area is determined interpolation after the excavation of the Mingyue Tunnels. Then, further correction and comprehensive values are taken according to the characteristics of underground river conduits.

2.4.4. Tunnels and underground river conduits

The underground river system consists of three karst branch conduits, which are located in three secondary karst trough valleys. To determine the characteristics of underground karst fractures, conduits and caves, geophysical prospecting was carried out by using magnetotelluric sounding (EH4), TEM, and the high-density resistivity method. Five magnetotelluric sounding profiles were created, each with a length of approximately 2 km, a point distance of 20 m and a depth of 650 m (Fig. 3). Then, the high-density resistivity method and TEM are used for correction. The formation lithology in the lower part of the survey line is determined according to the trend reflected by the resistivity chromatogram, and the karst characteristics or groundwater enrichment is judged according to the significant difference in resistivity between the center and both sides or the low-resistance closed circle. The spatial distribution of underground karst fractures, conduits and caves is shown in Table 2. The elevation of karst conduits in the western trough valley is 203 ~ 450 m, the elevation of karst conduits in the middle trough valley is 208 ~ 349 m, and the elevation of karst conduits in the eastern trough valley is 225 ~ 350 m. The lowest depth of karst conduits is in the middle trough valley, followed by the eastern trough valley and the western trough valley. The karst conduit in the middle trough valley should be considered the main conduit of the underground river system. The epikarst zone in the western trough valley is the largest.

To further explore the spatial distribution and scale of karst conduits and verify the interpretation results of geophysical prospecting, 26 hydrogeological boreholes were drilled around the three underground conduits (Fig. 3). The core from a borehole can directly reflect the

Table 2
Permeability coefficients of boreholes in the simulation area.

Number	Secondary trough valley	elevation(m)	Borehole depth (m)	Aquifer	Water level elevation (m)	Permeability coefficient K (m/d)
ZK1	West	421	251	T_1j^3	275.46	0.023
ZK2	West	470	260	T_1j^3	343.5	0.032
ZK3	Middle	520	302.8	T_1j、T_1d	410	0.018
DK1	Middle	497	258	T_1j^1	302.5	0.023
DK2	East	498	286	T_1j^1	289.57	0.024
DK3	East	540	180	T_1j^2	351.2	0.023
SW1	West	512.7	100	T_1j^1	482.2	0.014
SW2	Middle	523.2	130	T_1d	442.7	0.017
SW3	Middle	565	180.6	T_1d	422.4	0.011
SW4	East	513.7	150	T_1j^2	433.15	0.012
SW5	East	550.1	230.5	T_1d	403.51	0.012
SW6	West	575.9	315	T_1j^1	397.62	0.016
SW7	Middle	591.5	350	T_1j^1	338.21	0.025
SW9	West	514.5	270.6	T_1j^2	476.4	0.692
				T_1j^1 /T_1d		0.02 ~ 0.174
SW10	Middle	542.12	300.3	T_1d	395.4	0.021 ~ 0.181
SW11	East	536.9	300.5	T_1j^1	409.2	0.029 ~ 0.116
SW12	Middle	555.7	232	T_1j^1	391.3	0.018
SW13	West	493.9	190.85	T_1j^1	413.4	0.009 ~ 0.434
SW14	Middle	532.11	239.9	T_1d	368.46	2.34
SW15	East	544.17	211	T_1j^2	349.57	0.015
SW16	West	504.8	180.2	T_1j^2	465.9	1.507
				T_1j^1		0.388
SW17	West	463.46	170.8	T_1j^2	316.81	0.146
SW18	Middle	460.5	180.8	T_1j^2	325.3	0.118
SW19	East	524.7	210	T_1d	335.8	0.011
SW20	West	473.66	166.12	T_1j^2	365.31	0.027 ~ 1.145
SW21	Middle	555.7	273	T_1d	357.5	0.014

location and scale of underground karst conduits and caves (Fig. 4). According to the drilling records, karst caves and conduits are mainly present in the Jialingjiang Formation (T_1j) and decrease in abundance with increasing depth. From the recharge area to the discharge area, the elevations of karst caves and conduits are between 500 ~ 570 m, 400 ~ 460 m and 350 ~ 365 m.

The stable water level in boreholes can represent the regional groundwater level. Analysis of the water levels in the boreholes (Table 2) shows that the groundwater level in the western trough valley is higher than those in the middle trough valley and the eastern trough valley. In the runoff area, the groundwater level in the middle trough valley is higher than that in the eastern trough valley, while in the recharge area, the opposite is true.

In summary, based on hydrogeological surveys, geophysical prospecting, hydrogeological drilling and tests, the depth, scale and spatial distribution of karst caves, fracture zones and conduits are obtained. The elevation of the underground river conduit is 450 ~ 500 m (recharge area), 300 ~ 350 m (runoff area) and 180 ~ 250 m (discharge area). The permeability coefficients (k) near the underground river conduit are assigned according to the maximum values of the pumping test or regional empirical values, and then, they are simulated and verified according to the observation value of the water level in the borehole. Finally, the permeability coefficient (k) near the underground river conduit is inverted. The corrected values of the permeability coefficient at different depths in each stratum are shown in Table 3. The permeability coefficient (k) of the target layer is 0.25 ~ 0.72 m/d.

There are three tunnels in the simulation area, namely, the Chongqing-Wanzhou Railway Tunnels, Chongqing-Lichuan Railway Tunnels and Mingyue Tunnels. There is only a small amount of water seepage in the Chongqing-Wanzhou Railway Tunnels, which can be ignored. The drainage in the Chongqing-Lichuan Railway Tunnels is 17.514 ~ 27.524 L/s. According to the construction observation records of the Chongqing-Lichuan Railway Tunnels, there are three main water inflow sections. Three virtual boreholes are set in these water inflow sections, and the pumping capacity of a single borehole is approximately 400 ~ 1500 m^3/d. Similarly, seven virtual boreholes are set in the main water inflow sections of the Mingyue Tunnels, and the pumping capacity of a single borehole is approximately 100 ~ 1500 m^3/d. With the plugging of the water inflow section in the Mingyue Tunnels, the water inflow has decreased, and the pumping capacity of the borehole has decreased accordingly.

Table 3
Assignment of permeability coefficients to each stratum in the simulation area.

Position	Stratum	Main lithology	Permeability coefficient k (m/d)	
Two sides of the ridge	J_1zl	Mudstone, shale with sandstone	0.04	
	T_3xj^6	Sandstone and siltstone	0.15	
	T_3xj^5	Shale and siltstone with thin coal seam	0.04	
	T_3xj^4	Sandstone and siltstone	0.15	
	T_3xj^3	Shale and siltstone with thin coal seam	0.04	
	T_3xj^2	Sandstone and siltstone	0.15	
	T_3xj^1	Shale and siltstone with thin coal seam	0.04	
The western trough valley			Above 300 m	Below 300 m
	T_2l	Dolomitic limestone, dolomite and marl	0.45	0.35
	T_1j^3	Limestone and breccia	0.68	0.40
	T_1j^2	Limestone	0.48	0.35
	T_1j^1	Limestone and breccia	0.72	0.45
The middle trough valley			Above 300 m	Below 300 m
	T_1d	Limestone	0.45	0.25
	T_1f^4	Shale	0.05	0.05
	T_1f^3	Limestone	0.25	0.25
The eastern trough valley			Above 300 m	Below 300 m
	T_1j^1	Limestone and breccia	0.70	0.45
	T_1j^2	Limestone	0.45	0.35
	T_1j^3	Limestone and breccia	0.65	0.40
	T_2l	Dolomitic limestone, dolomite and marl	0.43	0.35

2.4.5. Modeling

Based on the 8 measured stratigraphic sections in the simulation area, virtual boreholes are set up at the intersection between the section and the main stratigraphic interface; thus, a 3D geological model of the model area is established (Fig. 5). In plan view, the simulation area is divided into 130 rows and 75 columns, with a total of 9750 grid cells.

2.4.6. Model calibration

Based on the hydrogeological parameters before and after tunnel excavation, the models before and after tunnel excavation are established respectively. To test the consistency between the temporal and spatial distribution of the groundwater flow field in the initial model and

a. SW9 b. SW11 c. SW10

Fig. 4. Core cComparison of borehole cores.

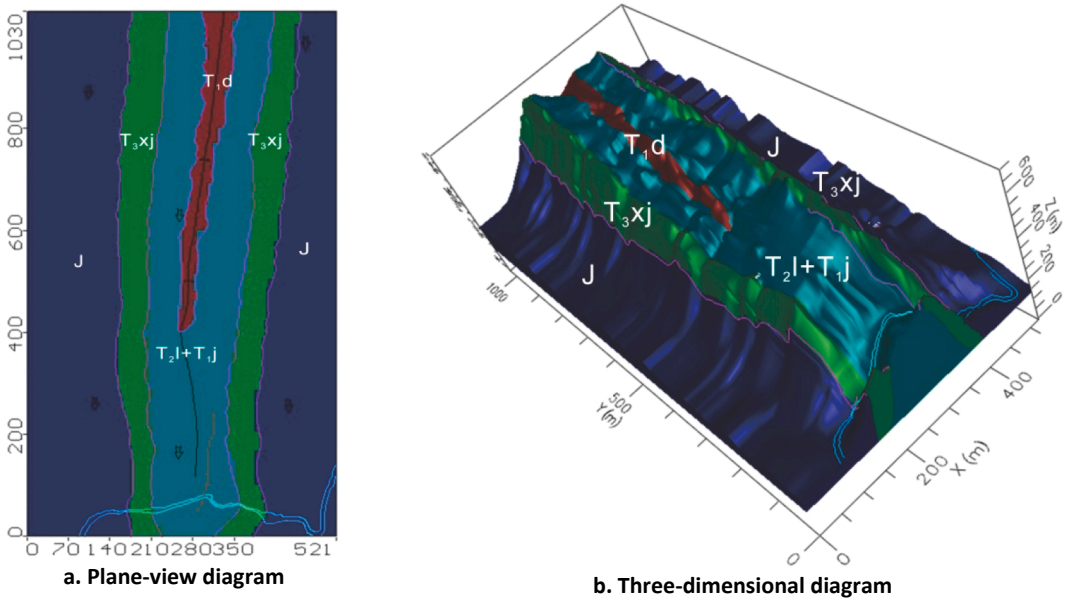

a. Plane-view diagram

b. Three-dimensional diagram

Fig. 5. Sketch of boundary conditions in the simulation area.

the measured value, model calibration is needed. The water levels in boreholes ZK1 ~ ZK3 and DK1 ~ DK3 before excavation of the Mingyue Tunnels are selected as the reference values for model calibration, and the water levels in boreholes ZK1 ~ ZK3 and SW5 ~ SW21 after Mingyue Tunnel excavation are selected as the reference values for model calibration. The best fitting effect can be obtained by simulating the operation and properly adjusting the parameters. The deviation error and fitting curve between the observed and simulated water levels of boreholes ZK1, ZK2 and ZK3 are shown in Fig. 6. The mean value of the residual error between the observed value and the simulated value is 0.202 ~ 0.208 m, indicating that the fitting degree of the model is good. In the simulation process, there is no obvious trend of error accumulation and expansion, which shows that the mathematical model is reliable.

3. Results

3.1. Tunnel drainage

As shown in Fig. 2 and Fig. 7, during the construction period of the Mingyue Tunnels (March 2018 ~ October 2020), the maximum total drainage was 25 L/s, and the drainage was 9.43 L/s. The drainage in carbonate rock was greater than that in clastic rock. The drainage of the right line (Entrance 2 and Exit 2) was greater than that of the left line (Entrance 1 and Exit 1). The tunnel drainage in the western trough valley and middle trough valley was high. Within one year after the completion of the Mingyue Tunnels (November 2020 ~ October 2021), the maximum total drainage was 20.14 L/s, and the average was 10.85 L/s.

The drainage of the Mingyue Tunnels shows a precipitation effect and karst conduit effect. The tunnel drainage in the rainy season accounts for more than 70% of the drainage over an entire year. However, when the tunnel exposes karst conduits (P1 and P2), the conduit effect is significant. For example, the precipitation in August and December 2019 was 18.1 mm and 26.9 mm, respectively, but the tunnel drainage was as high as 22.22 L/s and 17.01 L/s. The proportion of the drainage of the Mingyue Tunnels to the discharge of the underground river (S1) is high in the dry season and low in the rainy season. The proportions were 0.9%, 1.77% and 3.09% in the rainy season (June ~ September) from 2019 to 2021 and 3.97%, 6.89% and 9.37% in the dry season. Obviously, the drainage effect of the tunnel is stronger in the dry season than in the rainy season.

3.2. Changes in water level and quantity of surface water and groundwater

As shown in Fig. 8, the water levels and discharges of surface ponds SH1 and SH2, epikarst springs (S2, S3, S4, S6 and S7), borehole ZK1 and Chongqing-Lichuang Railway Tunnel F1 decreased due to the Mingyue Tunnel excavation. Other monitored springs or underground rivers exhibited no obvious changes.

The water levels of the two ponds (SH1 and SH2), which are 100 m south and 360 m north of the Mingyue Tunnels in the western trough valley, decreased significantly by 0.69 ~ 2.45 m from 2018 ~ 2020, while the water level of the two ponds (SH3 and SH4) that are far away from the tunnel changed with precipitation. When the drainage of the Mingyue Tunnels suddenly increased, the water levels of the two ponds did not decrease significantly. Therefore, tunnel drainage was not from surface water, and the changes in surface water might be due to the blasting vibration during tunnel excavation, which created cracks that penetrated to the bottom of the ponds, resulting in the leakage of surface water.

During the Mingyue Tunnel excavation, the discharges of S2 in the eastern trough valley and S4 in the middle trough valley almost dried up, and the discharges of S3, S6 and S7 in the western trough valley decreased by more than 50%. The discharges of these five springs decreased in the early stage of tunnel excavation, when the tunnel drainage was low. This might be due to the blasting vibration of tunnel excavation and the increase in water diversion cracks, resulting in the leakage of spring water. Within one year after the Mingyue Tunnels were completed (November 2020 ~ October 2021), three springs (S3, S6 and S7) fluctuated significantly with precipitation, and the discharges had recovered to near the levels observed prior to the construction period.

The discharge of the underground river and the water level of the three skylights (Y1, Y2 and Y3) did not drop significantly. The discharge of the underground river fluctuated greatly during the year, so it was difficult to judge the change in the underground river only from the discharge in a short period of time. However, the discharge of a karst conduit (P1) exposed by tunnel excavation after rain was 11.1 L/s. Therefore, it was inferred that the underground river system had been affected, resulting in a decrease in outlet discharge.

The water level of the borehole (ZK1) above the Mingyue Tunnels

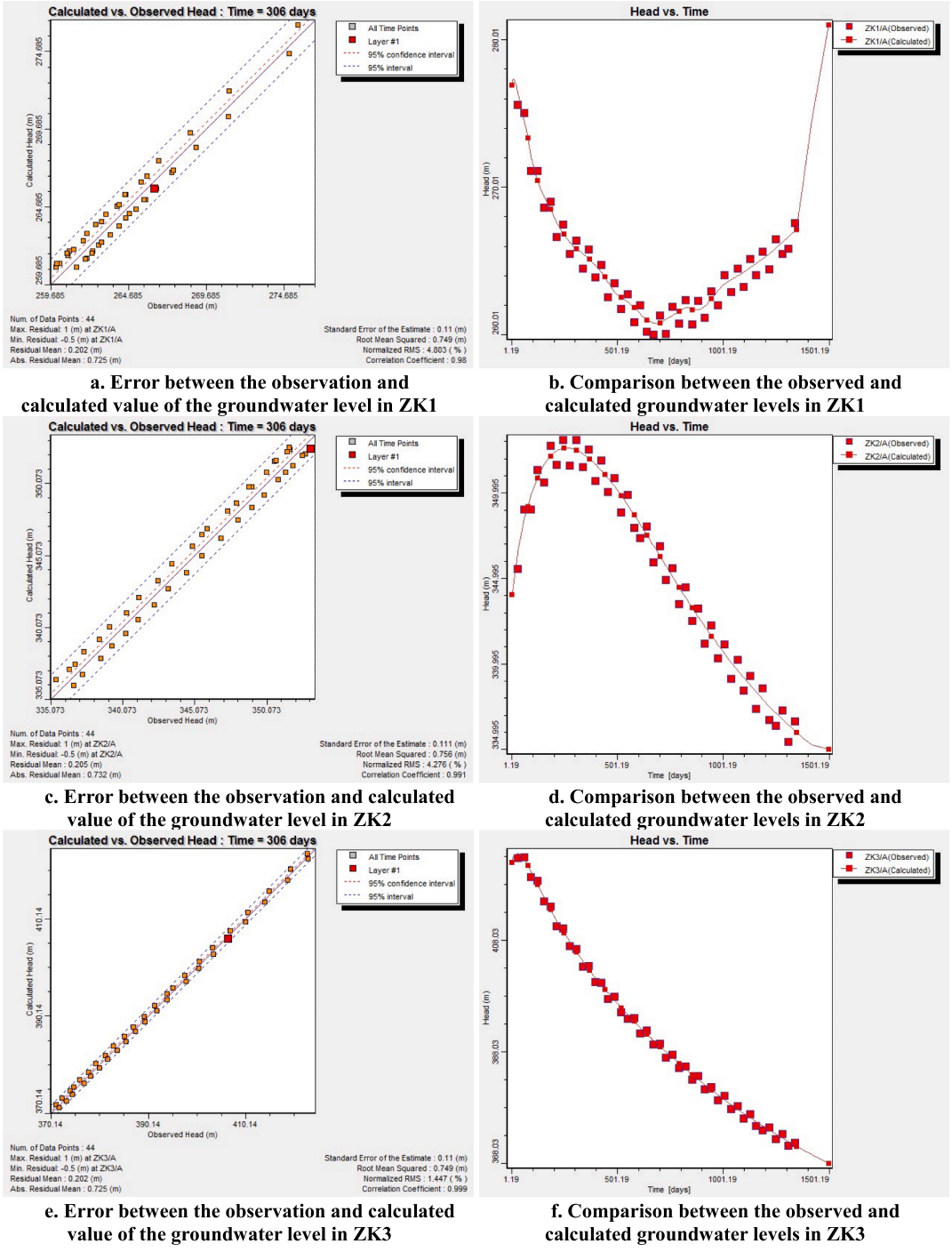

a. Error between the observation and calculated value of the groundwater level in ZK1

b. Comparison between the observed and calculated groundwater levels in ZK1

c. Error between the observation and calculated value of the groundwater level in ZK2

d. Comparison between the observed and calculated groundwater levels in ZK2

e. Error between the observation and calculated value of the groundwater level in ZK3

f. Comparison between the observed and calculated groundwater levels in ZK3

Fig. 6. Model calibration.

decreased by approximately 20 m at the beginning of tunnel excavation (March 2018) and then slowly decreased. The water level change in the borehole was not correlated with precipitation or tunnel drainage. Therefore, the sudden decrease in the water level might have been caused by blasting vibration during tunnel excavation. The water levels of the other five boreholes did not change significantly due to blasting vibration and tunnel drainage, and the seasonal variation range was 3.13 ~ 8.60 m.

The water inflow of the Chongqing-Lichuan Railway Tunnel, 1700 m south of the Mingyue Tunnels, has decreased since June 2018. The water inflow has decreased by 6 ~ 8 L/s in the rainy season and 2 ~ 3 L/s in the dry season, and the seasonal variation has also decreased. In June 2018 and July 2019, the drainage of the Chongqing-Lichuan Railway Tunnel decreased greatly, while the water inflow of the Mingyue Tunnels (Entrance 2) increased by 3.6 L/s and 8.33 L/s, respectively, compared with that of the previous month. The Chongqing-Lichuan Railway Tunnel crosses the Mingyue Tunnels in plane view and is 15 ~ 30 m higher than Mingyue Tunnels vertically. Therefore, the Mingyue Tunnels might capture part of the supply previously entering the Chongqing-Lichuan Railway Tunnel and cause some of the water to escape via leakage along cracks induced by blasting vibration.

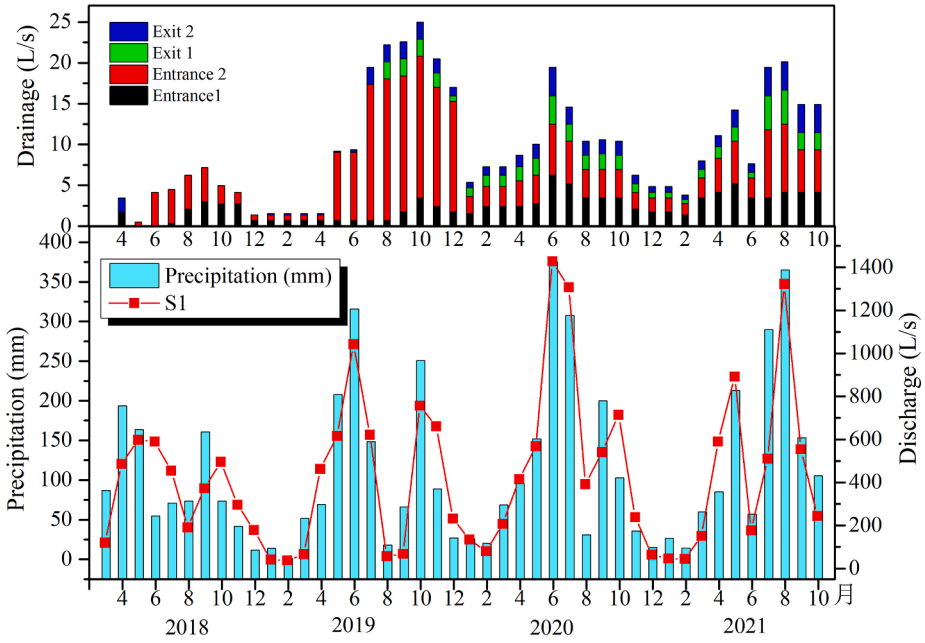

Fig. 7. Dynamic characteristics of drainage in the Mingyue Tunnels.

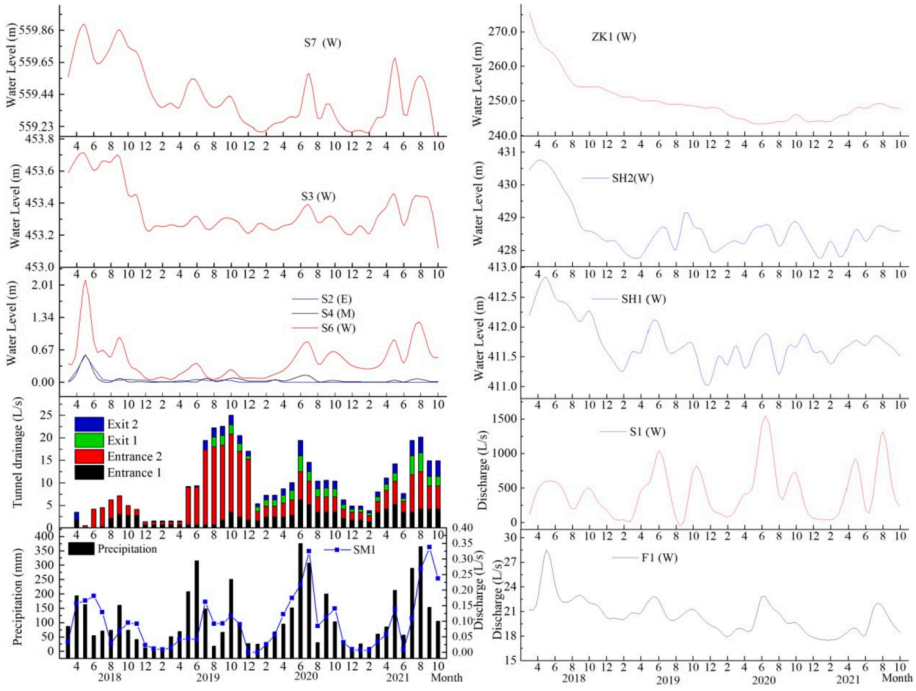

Fig. 8. Dynamic characteristics of the water level and quantity of surface water and groundwater.

3.3. Variation in the groundwater flow field

The karst groundwater flow fields before and after the excavation of the Mingyue Tunnels are shown in Fig. 9. Before tunnel excavation (Fig. 9a), the groundwater flow field in the simulation area was mainly controlled by the underground river, and the groundwater level gradually decreased from north to south, showing the pipeline catchment effect near the underground river pipeline. The water level in some sections (water level 310 ~ 250 m) was abnormal. Therefore, it is speculated that there was a local groundwater flow system. The hydraulic gradient at the intersection of the underground river and the Chongqing-Lichuan Railway Tunnel was large, which was due to the drainage effect of the Chongqing-Lichuan Railway Tunnel, forming a small depression cone. Additionally, the gradients of the karst conduits were large.

By the end of 2019, the two tunnels on the western side had passed through the western trough and entered the middle trough, while the two tunnels on the eastern side had not yet entered the carbonate rock stratum, and the water inflow in the western side tunnel was significantly greater than that in the eastern side. The karst groundwater flow field is shown in Fig. 9b. There is a small depression cone in the western trough valley and the middle trough valley, and the groundwater level in the depression cone is 30 m and 10 m lower than that in the surrounding area. There is a drawdown of 10 ~ 25 m near the axis of Mingyue

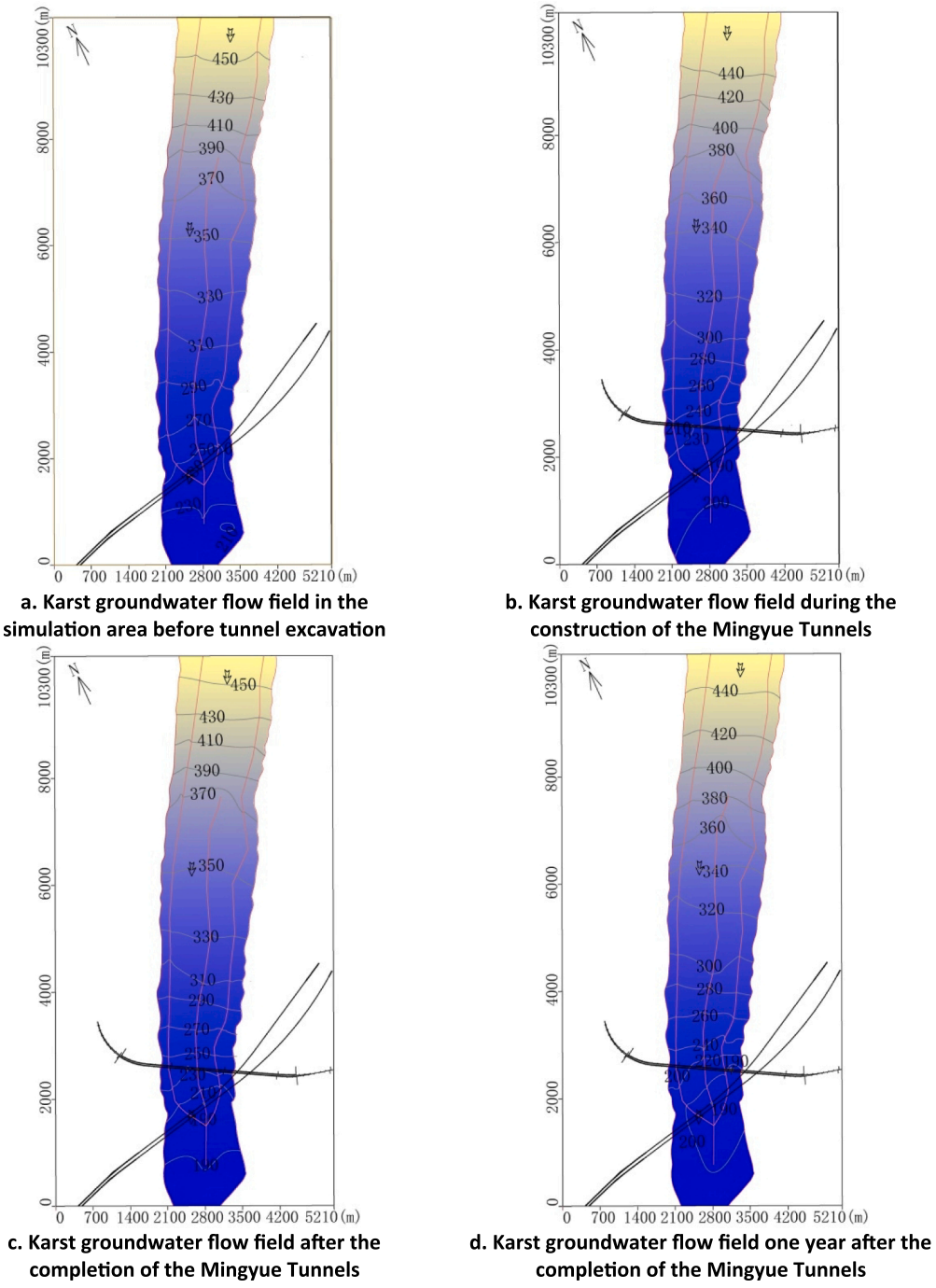

Fig. 9. Changes in the karst groundwater flow field.

Tunnels, and the decline range of the groundwater level decreases from the tunnel to the north and south sides. The hydraulic gradient in the tunnel site area increases. There is no depression cone in the eastern trough valley, but the groundwater level has relatively consistent changes with the middle trough valley and the western trough valley, which also proves that although the karst conduits in each secondary trough valley are independent of each other, they belong to the same underground river system and have a relatively unified groundwater surface. In the horizontal direction, the main influence range is 2 ~ 3 km from the north and south sides of the Mingyue Tunnels.

In October 2020, the Mingyue Tunnels were completed. The karst groundwater flow field is shown in Fig. 9c. There was a drawdown of 5 ~ 10 m near the axis of Mingyue Tunnels in 2020 compared with 2019. Due to the decline in the surrounding water level, the depression cone in the middle trough valley disappeared. In October 2021, one year after the tunnel was completed, the drainage of Mingyue Tunnels tended to be stable, and the area and depth of several depression cones increased. At the intersection of the Mingyue Tunnels, the Chongqing-Lichuan Railway Tunnel and the underground river, a depression zone is formed, and the groundwater level is approximately 10 m lower than that in the surrounding area, which may be due to the superposition effect of tunnel drainage and conduit catchments. The pattern of the groundwater flow field in other areas shows little change (Fig. 9d).

There are two main changes in the groundwater flow field caused by the drainage of Mingyue Tunnels: one is the formation of depression zones, which mainly appear near several water inflow points of the

tunnel. Due to the continuous water inflow (similar to the continuous pumping of pumping wells), the surrounding groundwater cannot be replenished in time, resulting in a depression zone, and the groundwater level in the depression zone will drop sharply. The hydraulic gradient increases sharply, and the flow velocity increases greatly. The second main change is the drawdown. The Mingyue Tunnels are near the discharge area of the groundwater system. The tunnel seizes the recharge water source of the underground river and forms an artificial groundwater discharge outlet, resulting in the drawdown and the change in the flow field in this hydrogeological unit.

3.4. Groundwater flow budget

The groundwater flow budget calculation using the above model suggests that the tunnels excavation results in a slight decrease in the groundwater storage in the study area. During the tunnel construction period, the net loss of groundwater storage in the hydrogeological unit is about 6.1×10^5 m^3, and the net loss of groundwater storage is about 1.7×10^5 m^3 one year after the tunnels were completed. Before the excavation of Mingyue Tunnels, the underground water in the hydrogeological unit was mainly discharged through underground river conduits and the Railway Tunnel. After the excavation of Mingyue Tunnels, they become new groundwater discharge outlets. The drainage of the Mingyue Tunnels accounted for 0.9% ~ 9.37% of the underground river (S1) discharge from 2019 to 2021, which may result in a reduction in underground river discharge. As shown in the Fig. 10, the predicted discharge of the underground river (S1) by the above model is in good agreement with the measured discharge. The discharge of underground river (S1) fluctuates obviously with precipitation. The simulated discharge in dry season is slightly less than the measured flow. When the tunnel drainage increases significantly in the rainy season in 2019 and 2020, the simulated underground river (S1) discharge is less than the measured flow.

4. Discussion

4.1. Impact of tunnel drainage on the groundwater flow field and groundwater resources

4.1.1. Judgment of the relative position of Mingyue Tunnels and underground river conduits

The records of tunnel construction and drainage show that large underground river conduits were not exposed during tunnel excavation. Therefore, the main conduits of the underground river should be below the Mingyue Tunnels within the seasonal variation zone of groundwater, and the underground river conduit of the western trough valley should be closer to the Mingyue Tunnels. The main evidence is as follows:

First, evidence from geophysical prospecting and hydrogeological drilling shows that the location and water level of the underground river conduit in the western trough valley are higher than those in the eastern and middle trough valleys, and the connectivity of the karst groundwater system is better. Therefore, the underground river conduit in the western trough valley is closest to the Mingyue Tunnels and is most vulnerable to the influence of tunnel excavation.

Second, according to the water level difference and distance between the skylight (Y3) and the outlet of the underground river in the dry season, the average hydraulic gradient of the underground river in the western trough valley is calculated to be 2.5%. Based on this calculation, the water level of the underground river in the western trough valley near the tunnel site area in the dry season is approximately 227.5 m, while the elevation of the Mingyue Tunnels is 257.64 ~ 282.46 m. Therefore, the Mingyue Tunnels are above the groundwater level in the dry season in this area (Fig. 11).

Third, the tunnel excavation exposed two karst conduits (P1 and P2), and the groundwater flow from the karst conduit (P1) featured a discharge of 11.1 L/s after precipitation. The discharge of this karst conduit (P1) is very stable in the rainy season, while it dries up in the dry season, indicating that the Mingyue Tunnels are below the regional groundwater level.

Finally, the tunnel drainage had a significant response to precipitation. The precipitation in the dry season is low, but the tunnel still has relatively stable drainage. The tunnel drainage was 3.82 ~ 4.21 L/s in

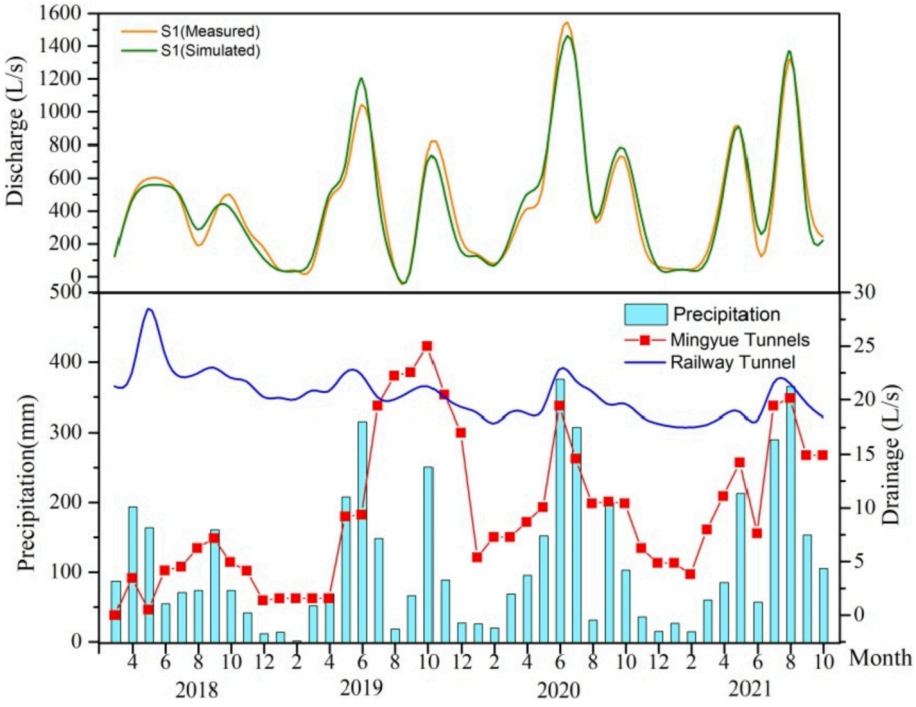

Fig. 10. Variations of underground river tunnel discharge after tunnel excavation.

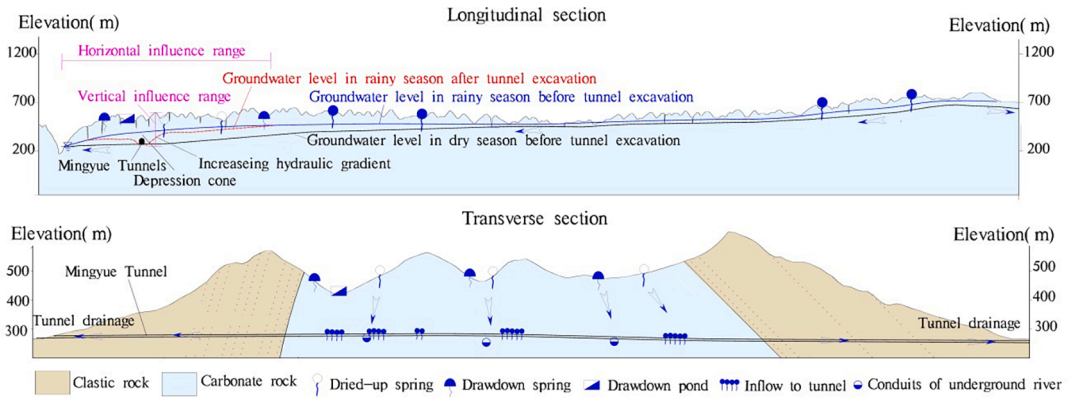

Fig. 11. Influence model of Mingyue Tunnels excavation on the groundwater flow field.

the dry season after the tunnel was connected, and it accounts for 8.63 ~ 10.72% of the underground river discharge in the dry season, indicating that the tunnel should be near the groundwater level in the dry season (Fig. 11).

4.1.2. Impact mode and mechanism

Due to the excavation of Mingyue Tunnels, the water levels of two surface ponds (SH1 and SH2), the water level of a borehole (ZK1), and the discharge of three epikarst springs in the western trough valley decreased; the discharge of an epikarst spring S4 in the middle trough valley and an epikarst spring S2 in the eastern trough valley decreased. The discharge of surface karst springs (S3, S6 and S7) gradually recovered after the Mingyue Tunnels were connected. Therefore, it is speculated that during tunnel excavation, the northern boundary of the horizontal influence range was 7100 m (S7) from the Mingyue Tunnels, the southern boundary was 1700 m (underground river outlet S1) from the Mingyue Tunnels, and the east–west influence range was between the tunnel entrance and exit. The groundwater flow field simulation shows that the impact is relatively serious within 2 km of the Mingyue Tunnels on both sides. Vertically, the influence range should be from the ground to the bottom of the Mingyue Tunnels (257.64 ~ 282.46 m), and it gradually decreases from the tunnel site to the north and south.

The drainage of the Mingyue Tunnels has both precipitation and conduit effects. During tunnel excavation, the drainage in the rainy season accounted for 65.49% ~ 75.41% of the annual drainage, while the drainage in the dry season accounted for only 24.59% ~ 34.51%. In July and September 2019, when two karst conduits (P1 and P2) were exposed during the excavation of the Mingyue Tunnels, the conduit effect of tunnel drainage was significant. From July to October 2019, the tunnel drainage was 17.01 ~ 25.0 L/s, which was the maximum drainage during the excavation and was not affected by the precipitation. After the completion of the Mingyue Tunnels, the tunnel drainage no longer had a conduit effect. It is speculated that the tunnel drainage reduced the groundwater level, and the groundwater level in the rainy season was lower than that of karst conduit P1 before tunnel excavation.

There are significant temporal and spatial differences in the impact of Mingyue Tunnel drainage on the groundwater flow field. From 2019 to 2021, the tunnel drainage in the rainy season accounted for 0.9% ~ 3.09% of the underground river (S1) discharge in the same period, while the tunnel drainage in the dry season accounted for 3.97% ~ 9.37%. Therefore, the tunnel drainage effect is stronger in the dry season. Precipitation recharge in the rainy season can alleviate the decline in the groundwater level caused by tunnel excavation. Groundwater resources in karst areas are unevenly distributed in their natural state. The maximum discharge of underground rivers in the rainy season is usually dozens of times that in the dry season, and the water level may differ by tens of meters. The tunnel drainage aggravates the spatial–temporal distribution differences in water resources. Among all kinds of surface water and underground water bodies monitored, the most obvious drainage changes were in the Chongqing-Lichuan Railway Tunnel adjacent to the Mingyue Tunnels, followed by the epikarst springs and ponds. The underground river system was also affected, but not significantly, due to the small proportion of tunnel drainage for underground river discharge. Although 6 boreholes were monitored, only the water level of borehole ZK1 above the Mingyue Tunnels was affected by tunnel drainage. The impact of tunnel drainage on the groundwater system in the western trough valley is greater than that in the middle trough valley and the eastern trough valley. There are more epikarst springs, sinkholes, and underground river skylights in the western trough valley, and the connectivity of the groundwater system is better. The conduits of the underground river and groundwater level in the western trough valley are higher, and thus, the response to the drainage via the Mingyue Tunnels is stronger. The water bodies south of the Mingyue Tunnels are more obviously affected by the tunnel drainage. The outlet of the underground river, epikarst spring S2, pond SH1 and the exit of Chongqing-Lichuan Railway Tunnel F1 are all south of the Mingyue Tunnels, and karst conduit P1 is mainly discharged from the southern section. This difference is mainly because the monitoring water bodies in the south are close to the Mingyue Tunnels, and the Mingyue Tunnels also intercepted the recharge water source of the southern groundwater body.

There are two ways in which tunnel excavation affects the groundwater flow field. One is the blasting vibration induced by tunnel excavation, which leads to the expansion of karst fractures or the generation of new fractures, destroys the aqueous medium, and leads to the leakage of some shallow groundwater and surface water into the tunnel (Fig. 11). The reduction in shallow water resources will affect groundwater-dependent ecosystems (Liu et al., 2019). Second, the tunnel excavation exposed karst conduits, resulting in the groundwater once flowing through these conduits being directly discharged into the tunnel, the groundwater level dropping below the conduit, the underground river system being damaged, and the tunnel becoming a new groundwater outlet. In the long term, the karstification process can even be altered, which in turn may amplify or weaken the effects of climate on vegetation growth (Jiang et al., 2020).

4.2. Influence of tunnel location on its drainage effect

The location of the tunnel directly affects the amount of drainage, so it is the most important factor that changes the groundwater flow field. Vertically, although some tunnels in karst mountains may start in the vadose zone at each end, they may pass into a transient zone or even a steady-state phreatic zone in their central parts, creating an elongated zone of depression that permits gravity-driven drainage and resulting in a lowered groundwater level (Ford and Williams, 2007; Vincenzi et al., 2009) and the drying up of springs and even underground rivers, if

tunnels are excavated above the low groundwater level (in the dry season) in karst areas, and if the tunnel is located below the high groundwater level (in the rainy season), some epikarst springs may be drained, and the shallow groundwater in the aeration zone may be reduced. Horizontally, if the tunnel is located in the recharge area and is near the surface, it may affect only the epikarst springs around the recharge area, resulting in a slight decrease in underground river discharge downstream, while not affecting the epikarst springs downstream. If the tunnel is located in the groundwater discharge area and is deep, there will be a large drawdown, which can affect the whole groundwater system.

There was no abrupt decrease in the groundwater level or severe drainage of the underground river after the excavation of the Mingyue Tunnels, mainly due to the relatively high position of the tunnel. As mentioned above, the Mingyuen Tunnels are at the bottom of the seasonal variation zone, that is, above the water level in the dry season and below the water level in the wet season, close to the dry-season water level. Assuming that the tunnel is below the low water level in the dry season, the tunnel drainage may increase several times. According to the drainage of several water inflow points in the Mingyue Tunnels estimated based on the discharge of the underground river in the dry season, the groundwater flow field of this hydrogeological unit is reconstructed when the Mingyue Tunnels are below the groundwater level in the dry season (Fig. 12). When the Mingyue Tunnels were completed in October

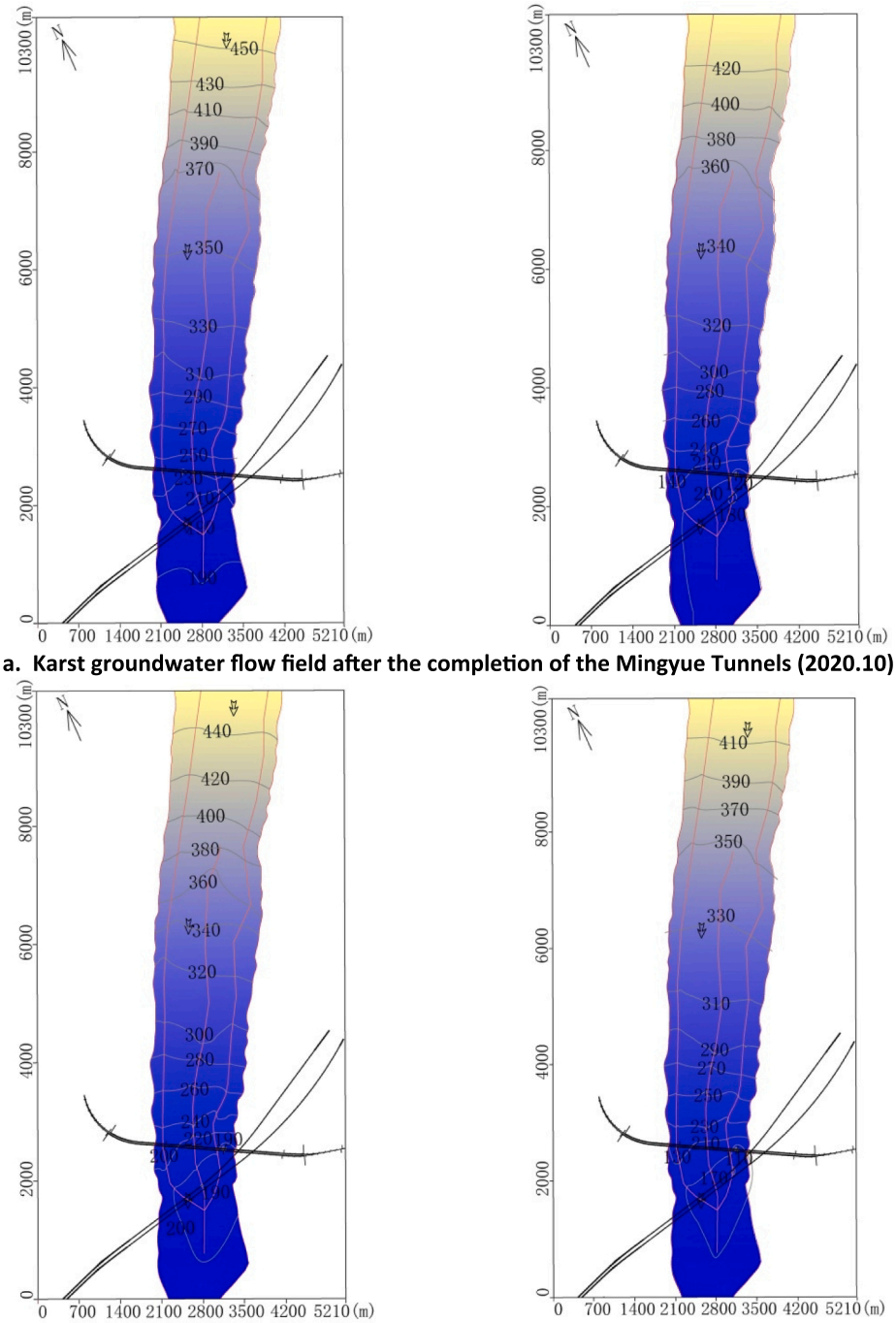

a. Karst groundwater flow field after the completion of the Mingyue Tunnels (2020.10)

b. Karst groundwater flow field one year after the completion of the Mingyue Tunnels (2021.10)

Fig. 12. Variation in the karst groundwater flow field when the Mingyue Tunnels are in horizontal groundwater runoff. The tunnel on the left is above the water level in the dry season, and the tunnel on the right is below the water level in the dry season.

2020, compared with the groundwater flow field when the tunnels are above the groundwater level in the dry season, the area of several depression cones near the axis of Mingyue Tunnels expanded by 2 ~ 3 times, the depth increased by 30 ~ 70 m, the catchment effect at the intersection of the Chongqing-Lichuan Railway Tunnel and the underground river strengthened, and the hydraulic gradient of groundwater increased. The horizontal influence range of the Mingyue Tunnel drainage expanded from 3 km to 8.0 km. One year after the completion of the Mingyue Tunnels in October 2021, compared with the groundwater flow field when the tunnel is above the groundwater level in the dry season, the depth of several depression cones near the axis of the Mingyue Tunnel increased by 20 ~ 80 m, the catchment effect at the intersection of the Chongqing-Lichuan Railway Tunnel and the underground river was stronger, and the hydraulic gradient of groundwater and the scope of influence were larger.

4.3. *Influence of precipitation on the tunnel drainage effect*

The main source of recharge in the study area is precipitation. In the natural state, the response of the groundwater level and underground river discharge to precipitation is very significant. Considering the interference of tunnel, variations of the tunnel drainage, the groundwater level near the tunnel and the flow of underground river (S1) under different precipitation conditions are predicted (Fig. 13).

When the annual precipitation increases by 200 mm, the drainage of Mingyue Tunnels in dry season increase by 15%~59%, with an average increase of 35%, and the drainage of Mingyue Tunnels in rainy season increase by 3%~23%, with an average increase of 10%; when the annual precipitation increases by 400 mm, the drainage of Mingyue Tunnels in dry season increase by 19% ~62%, with an average increase of 38%, and the drainage of Mingyue Tunnels in rainy season increase by 14%~35%, with an average increase of 21% (Fig. 13a). The drainage of Mingyue Tunnels responds more significantly to precipitation in dry season, which is consistent with the previous observation results.

When the annual precipitation increases by 200 mm, the groundwater level near Mingyue Tunnels increases by 5%~7% in dry season, with an average increase of 6%, and the groundwater level near Mingyue Tunnels increases by 5% in rainy season; when the annual precipitation increases by 400 mm, the groundwater level near Mingyue Tunnels increases by 13%~14% in dry season, with an average increase of 14%, and the groundwater level near Mingyue Tunnels increases by 10%~11% in rainy season, with an average increase of 11% (Fig. 13b).

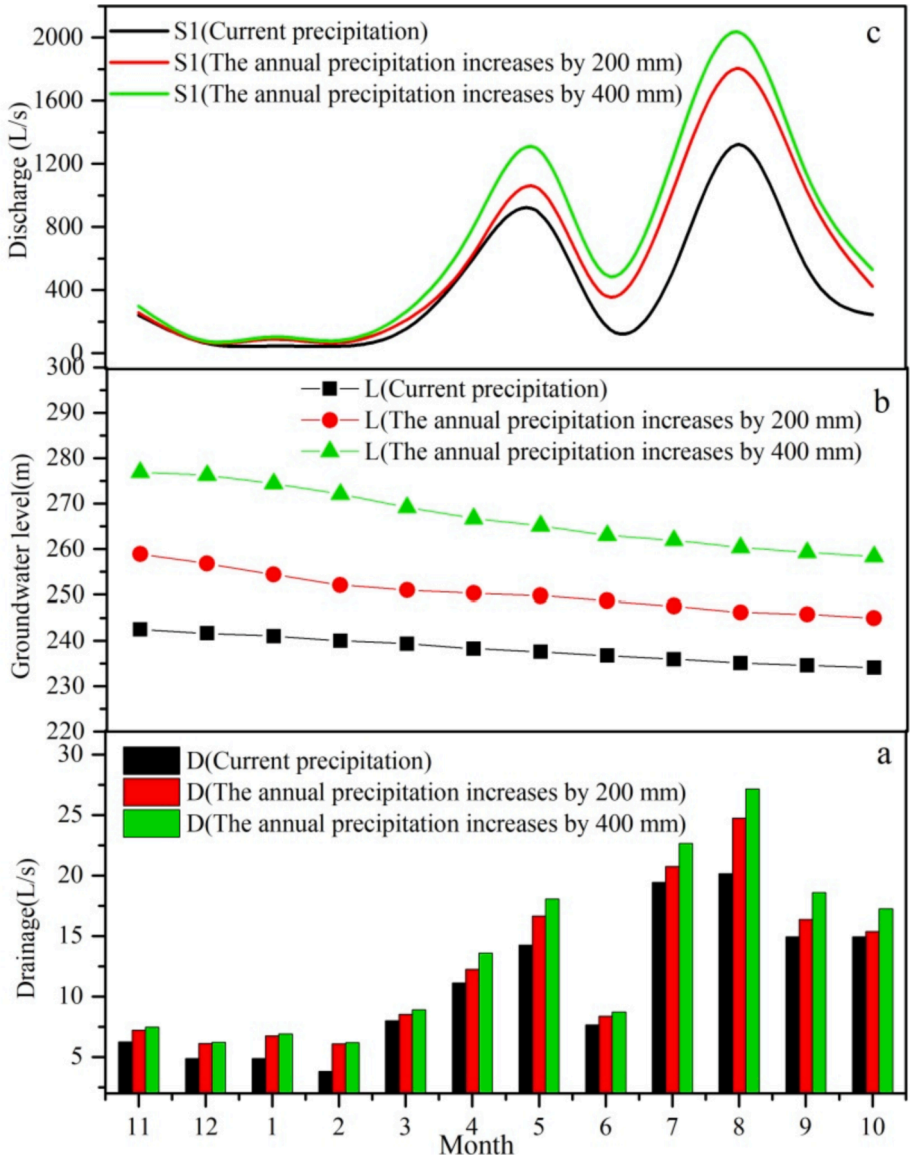

Fig. 13. Prediction of the underground river discharge, groundwater level and tunnel drainage under different precipitation conditions.

The annual average groundwater level near the Mingyue Tunnels rises up by 12.46 m and 16.42 m respectively with the increase of precipitation. However, the increase of precipitation promotes the underground river discharge and tunnel drainage, resulting in the drawdown of groundwater level near the tunnel in the same period, and the drawdown is greater in rainy season than that in dry season. Therefore, the groundwater level near the tunnel in rainy season is lower than that in dry season, which is significantly different from that in natural state.

When the annual precipitation increases by 200 mm, the discharge of underground river (S1) in dry season increases by 7%~94%, with an average increase of 40%, and the discharge of underground river (S1) in rainy season increases by 36%~106%, with an average increase of 81%; when the annual precipitation increases by 400 mm, the discharge of underground river (S1) in dry season increases by 20%~125%, with an average increase of 62%, and the discharge of underground river (S1) in rainy season increases by 54%~182%, with an average increase of 120% (Fig. 13c). Under the interference of Mingyue Tunnels, the discharge of underground river (S1) still responds significantly to the increase of precipitation, and the increase in rainy season is greater than that in dry season. When the precipitation increases by 200 mm and 400 mm respectively, the average discharge ratio of the underground river in rainy season and dry season increases from 5.7 to 7.76 and 7.82 respectively. As mentioned above, the drainage effect of tunnel is more significant in dry season, and the tunnel drainage accounts for a larger proportion of underground river discharge. Therefore, driven by the increase of precipitation and tunnel drainage, the seasonal variation of underground river discharge is exacerbated.

4.4. Recovery of groundwater resources

The prediction of groundwater flow budget shows that the net loss of groundwater storage is 1.7×10^5 m^3/a under the current precipitation conditions; the net loss of groundwater storage is 1.2×10^5 m^3/a when the annual precipitation increases by 200 mm; the net loss of groundwater storage is 0.5×10^5 m^3/a when the annual precipitation increases by 400 mm. The simulation prediction indicates that although the increase of precipitation raises the groundwater level and alleviates the drainage effect, there is still a loss of groundwater storage.

4.5. Limitations and improvement methods

Some limitations and improvement methods in this study are as follows:

First, the karst aquifer is heterogeneous, so the hydrogeological parameters vary greatly and will change due to tunnel interference. The detailed hydrogeological parameters before and after tunnel excavation are the most important factor for the success of modeling. In this study, 8 geological profiles were measured, and the real thicknesses of the strata in the simulation area were obtained. The discharges of 10 springs in the dry season were measured twice, and the precipitation infiltration coefficients before and after tunnel excavation were obtained. Three geophysical prospecting methods and twenty-six hydrogeological boreholes were used to confirm the distribution and elevation of underground karst fractures, conduits and caves. More than 26 pumping tests and water pressure tests were carried out before and after tunnel excavation, and the hydrogeological parameters before and after tunnel excavation were obtained. The model is calibrated by using the water level observation data before and after tunnel excavation to ensure the effectiveness of the model.

Second, Visual MODFLOW assumes that the flow field is continuous and that flow movement obeys Darcy's law, and it is not an ideal model to simulate karst groundwater flow. Some efforts have been made to solve the contradiction between the heterogeneity in karst aquifers and the assumptions of the model. A large number of hydrogeological parameters are obtained before and after tunnel excavation. Then, due to the heterogeneity in the karst aqueous medium, different parameters are assigned to different karst conduits with different elevations. Based on abundant observed water level data before and after tunnel excavation, the model is modified, and the hydrogeological parameters are inverted to establish a more realistic groundwater flow field.

Finally, due to the limitations of the model, the water exchange between underground river and conduits with metrix is not considered. This study improves the accuracy of simulation by increasing hydrogeological tests and obtaining more hydrogeological parameters.

5. Conclusion and prospects

Thirty-four surface ponds, springs, underground rivers and boreholes were monitored in a karst trough valley in Southwest China, and Visual MODFLOW was used to simulate, predict and calculate the groundwater flow field and discharge; thus, the change in the groundwater flow field and the discharge of the underground river were revealed, and then the hydrogeological impact of tunnel excavation on the karst groundwater aquifer was quantitatively evaluated.

Observation and simulation indicate that tunnel excavation has a differential impact on groundwater flow field and discharge. The drainage effect of tunnel is more significant in dry season. The underground system in the western trough valley responds more strongly to the tunnel drainage. The surface water level dropped by 0.69 ~ 2.45 m, the discharge of five epikarst springs dropped abruptly or almost drained. The drainage of the Chongqing-Lichuan Railway Tunnel decreased by approximately a quarter, and the groundwater level of the borehole dropped by approximately 20 m. The northern and southern boundaries of the horizontal influence range were 7100 m and 1700 m from the Mingyue Tunnels, respectively. Vertically, the influence range extends from the ground to the bottom of the Mingyue Tunnels. There is a drawdown of 10 ~ 30 m due to the excavation of the Mingyue Tunnels.

The simulation results predict that the drainage effect is more significant when the tunnels are below the groundwater level in the dry season. Driven by the increase of precipitation and tunnel drainage, the seasonal variation of underground river discharge is exacerbated. The increase of precipitation promotes the underground river discharge and tunnel drainage, resulting in the drawdown of groundwater level near the tunnel in the same period. Therefore, the groundwater level near the tunnel in the rainy season is lower than that in the dry season, which is opposite to that in natural state.

The groundwater flow budget calculation and prediction suggest that the net loss of groundwater storage was 6.1×10^5 m^3 during tunnel excavation, and the net loss of groundwater storage is about 1.7×10^5 m^3 one year after the tunnels were completed, while the depression cones continue to expand. The net loss of groundwater storage is 1.2×10^5 m^3/a and 0.5×10^5 m^3/a when the annual precipitation increases by 200 mm and 400 mm respectively. The increase of precipitation raises the groundwater level and alleviates the drainage effect, but the increased precipitation recharge is less than groundwater discharge and tunnel drainage, and there is still a loss of groundwater storage. So it is difficult to restore the groundwater flow field and discharge in a short time.

This study provides evidence and a useful method to quantitatively evaluate the effects of tunnel excavation on the groundwater flow field and to inform better measures to protect karst groundwater resources. In the future, we will continue to observe the groundwater level and hydrochemical characteristics around the completed Mingyue Tunnels to study the recovery process of the groundwater flow field.

CRediT authorship contribution statement

Yuxiang Lv: Data curation, Methodology, Software, Writing – original draft. **Jing Jiang:** Software, Validation. **Li Chen:** Visualization, Investigation. **Wei Hu:** Investigation. **Yongjun Jiang:** Conceptualization, Supervision, Writing – review & editing.

Declaration of Competing Interest

The authors declare that they have no known competing financial interests or personal relationships that could have appeared to influence the work reported in this paper.

Acknowledgments

This research was supported by the National Key Research and Developmental Program of China (2016YFC0502306, 2016YFC0502302) and the Chongqing Municipal Science and Technology Commission Fellowship Fund (cstc2019yszx-jcyjX0002, cstc2020yszx-jcyjX0006, cstc2021yszx-jcyjX0005).

References

Aliouache, M., Wang, X., Jourde, H., Huang, Z., Yao, J., 2019. Incipient karst formation in carbonate rocks: influence of fracture network topology. J. Hydrol. 575, 824–837.
Attanayake, P.M., Waterman, M.K., 2006. Identifying environmental impacts of underground construction. Hydrogeol. J. 14 (7), 1160–1170.
Butscher, C., Huggenberger, P., Zechner, E., 2011. Impact of tunneling on regional groundwater flow and implications for swelling of clay–sulfate rocks. Eng. Geol. 117 (3-4), 198–206.
Butscher, C., 2012. Steady-state groundwater inflow into a circular tunnel. Tunn. Undergr. Sp. Tech. 32, 158–167.
Cao, M., Wu, C., Liu, J.C., Jiang, Y.J., 2020. Increasing leaf $\delta^{13}C$ values of woody plants in response to water stress induced by tunnels excavation in a karst trough valley: Implication for improving water-use efficiency. J. Hydrol. 586.
Chang, Y., Wu, J., Liu, L., 2015. Effects of the conduit network on the spring hydrograph of the karst aquifer. J. Hydrol. 527, 517–530.
Chen, X., Zhang, Z., Soulsby, C., Cheng, Q., Binley, A., Jiang, R., Tao, M., 2018. Characterizing the heterogeneity of karst critical zone and its hydrological function: an integrated approach. Hydrol. Process 32 (19), 2932–2946.
Chen, Y.-F., Liao, Z., Zhou, J.-Q., Hu, R., Yang, Z., Zhao, X.-J., Wu, X.-L., Yang, X.-L., 2020. Non-Darcian flow effect on discharge into a tunnel in karst aquifers. Int. J. Rock Mech. 130, 104319.
Chiu, Y.-C., Chia, Y., 2012. The impact of groundwater discharge to the hsueh-shan tunnel on the water resources in northern taiwan. Hydrogeol. J. 20 (8), 1599–1611.
Coli, M., Pinzani, A., 2014. Tunnelling and hydrogeological issues: a short review of the current state of the art. Rock Mech. Rock Eng. 47 (3), 839–851.
El Tani, M., 2003. Circular tunnel in a semi-infinite aquifer. Tunn. Undergr. Sp. Tech. 18 (1), 49–55.
El Tani, M., 2010. Helmholtz evolution of a semi-infinite aquifer drained by a circular tunnel. Tunn. Undergr. Sp. Tech. 25 (1), 54–62.
Ford, D.C., Williams, P.W., 2007. Karst Hydrogeology and Geomorphology. Wiley, Chichester.
Gallegos, J.J., Hu, B.X., Davis, H., 2013. Simulating flow in karst aquifers at laboratory and sub-regional scales using MODFLOW-CFP. Hydrogeol. J. 21 (8), 1749–1760.
Gan, F.P., Yu, L.P., Li, H.Q., Lu, C.J., Wei, J.Y., 2010. Detection of groundwater conducts by integrated geophysical methods. Geol. Resour. 19 (3), 262–266.
Giese, M., Reimann, T., Bailly-Comte, V., Maréchal, J.-C., Sauter, M., Geyer, T., 2018. Turbulent and laminar flow in karst conduits under unsteady flow conditions: interpretation of pumping tests by discrete conduit-continuum modeling. Water Resour. Res. 54 (3), 1918–1933.
Gisbert, J., Vallejos, A., González, A., Pulido-Bosch, A., 2009. Environmental and hydrogeological problems in karstic terrains crossed by tunnels: a case study. Environ Geol. 58, 347–357.
Goodman, R.E., Moye, D.G., Schalkwyk, A., Javandel, I., 1965. Groundwater inflows during tunnel driving. Eng. Geol. 2 (1), 39–56.
Hadi, F., Arash, N.H., 2018. Water flow into tunnels in discontinuous rock: a short critical review of the analytical solution of the art. B. Eng. Geol. Environ. 78 (5), 3833–3849.
Hill, M.E., Stewart, M.T., Martin, A., 2010. Evaluation of the MODFLOW-2005 conduit flow process. GroundWater 48 (4), 549–559.
Hu, X., Wang, X., Gunzburger, M., Hua, F., Cao, Y., 2012. Experimental and computational validation and verification of the Stokes-Darcy and continuum pipe flow models for karst aquiferswith dual porosity structure. Hydrol. Process 26 (13), 2031–2040.
Jiang, G.H., Guo, F., Tang, Q.J., Li, X., Zeng, X.R., 2016. Application of artificial tracing technology in hydrogeological survey in karst area. J. Nanjing Univers. Natl. Sci. Ed. 52 (3), 9.
Jiang, Z., Liu, H., Wang, H., Peng, J., Meersmans, J., Green, S.M., Song, Z., 2020. Bedrock geochemistry influences vegetation growth by regulating the regolith water holding capacity. Nat. Commun. 11 (1), 2392.
Kim, Y.Y., Lee, K.K., Sung, I.H., 2001. Urbanization and the groundwater budget, metropolitan Seoul areas. Korea. Hydrogeol. J. 9, 401–412.
Koyama, T., Kogiso, J., Takahashi, K., Yasuda, T., Ohnishi, Y., 2012. Development of swing method with sequential data assimilation (SDA-SWING) and its application to groundwater problems in real tunnel construction. Tunn. Undergr. Sp. Tech. 28, 229–237.
Laura, K., RademacherJordan, F., ClarkJames, R., Boles, 2003. Groundwater residence times and flow paths in fractured rock determined using environmental tracers in the Mission Tunnel; Santa Barbara County, California. USA. Environ. Geol. 43 (5), 557–567.
Li, H.Q., Wei, J.Y., Lao, W., 2008. CT-between electromagnetic detection revealed reservoir dam foundation karst morphological characteristics-Gangxi Jingxi in the Longtan curtain filling the reservoir as an example. Rock and Soil Mechanics 29 (z1), 607–610.
Li, J., Hong, A.H., Yuan, D.X., Jiang, Y.J., Deng, S.J., Cao, C., Liu, J.C., Liu, J., 2020. A new distributed karsttunnel hydrological model and tunnel hydrological effect simulations. J. Hydrol.
Liu, J., Shen, L., Wang, Z., Duan, S., Wu, W., Peng, X., Wu, C., Jiang, Y., 2019. CT detection of inter hole electromagnetic wave reveals the morphological characteristics of bedrock dissolution of reservoir dam. Rock and Soil Mechanics, 29, 607–610.Liu, J., Shen, L., Wang, Z., Duan, S., Wu, W., Peng, X., Wu, C., Jiang, Y., 2019. Response of plants water uptake patterns to tunnels excavation based on stable isotopes in a karst trough valley. J. Hydrol. 571, 485–493.
Liu, Z., Li, Q., Sun, H., Wang, J., 2007. Seasonal, diurnal and storm-scale hydrochemical variations of typical epikarst springs in subtropical karst areas of SW China: Soil CO_2 and dilution effects. J. Hydrol. 337 (1-2), 207–223.
Lv, Y., Jiang, Y., Hu, W., Cao, M., Mao, Y., 2020. A review of the effects of tunnels excavation on the hydrology, ecology, and environment in karst areas: Current status, challenges, and perspectives. J. Hydrol. 586, 1–15.
Maréchal, J.-C., Lanini, S., Aunay, B., Perrochet, P., 2014. Analytical solution for modeling discharge into a tunnel drilled in a heterogeneous unconfined aquifer. GroundWater 52 (4), 597–605.
Mastrocicco, M., Vignoli, G., Colombani, N., Zeid, N.A., 2010. Surface electrical resistivity tomography and hydrogeological characterization to constrain groundwater flow modeling in an agricultural field site near Ferrara (Italy). Environ. Earth. Sci. 61 (2), 311–322.
Moon, J., Jeong, S., 2011. Effect of highly pervious geological features on ground-water flow into a tunnel. Eng. Geol. 117 (3-4), 207–216.
Mossmark, F., Ericsson, L.O., Norin, M., Dahlström, L.O., 2015. Hydrochemical changes caused by underground constructions-A case study of the Kattleberg rail tunnel. Eng. Geol. 191, 86–98.
Kolymbas, D., Wagner, P., 2007. Groundwater ingress to tunnels -The exact analytical solution. Tunn. Undergr. Sp. Tech. 22 (1), 23–27.
Parsekian, A.D., Singha, K., Minsley, B.J., Holbrook, W.S., Slater, L., 2015. Multiscale geophysical imaging of the critical zone. Rev. Geophys. 53 (1), 1–26.
Park, K.H., Owatsiriwong, A., Lee, J.G., 2008. Analytical solution for steady-state groundwater inflow into a drained circular tunnel in a semi-infinite aquifer A revisit. Tunn. Undergr. Sp. Tech. 23 (2), 206–209.
Perrochet, P., 2005. Confined flow into a tunnel during progressive drilling: An analytical solution. GroundWater 43 (6), 943–946.
Raposo, J.R., Molinero, J., Dafonte, J., 2010. Quantitative evaluation of hydrogeological impact produced by tunnel construction using water balance models. Eng. Geol. 116 (3–4), 323–332.
Scheidler, S., Huggenberger, P., Butscher, C., Dresmann, H., 2019. Tools to simulate changes in hydraulic flow systems in complex geologic settings affected by tunnels excavation. Bull. Eng. Geol. Environ. 78, 969–980.
Shoemaker, W.B., Kuniansky, E.L., Birk, S., Bauer, S., Swain, E.D., 2008. Documentation of a conduit flow process (CFP) for MODFLOW-2005. Techniques & Methods, USGS, pp. 1–48.
Vincenzi, V., Gargini, A., Goldscheider, N., 2009. Using tracer tests and hydrological observations to evaluate effects of tunnel drainage on groundwater and surface waters in the Northern Apennines (Italy). Hydrogeol. J. 17 (1), 135–150.
Vincenzi, V., Gargini, A., Goldscheider, N., Piccinini, L., 2014. Differential Hydrogeological Effects of Draining Tunnels Through the Northern Apennines. Italy. Rock Mech. Rock Eng. 47 (3), 947–965.
White, W.B., 2007. A brief history of karst hydrogeology: contributions of the NSS. J. Cave Karst Stud. 69, 13–26.
Xia, Q., Xu, M., Zhang, H., Zhang, Q., Xiao, X.X., 2018. A dynamic modeling approach to simulate groundwater discharges into a tunnel from typical heterogenous geological media during continuing excavation. KSCE J. Civ. Eng. 22 (1), 341–350.
Zargham, M., Walter, A., Illman, M., 2018. Optimization of the hydrodynamic characteristics of a karst conduit with CFPv2 coupled to ostrich. J. Hydrol. 567, 564–578.
Zhang, W., Dai, B., Liu, Z., Zhou, C., 2019. On the non-Darcian seepage flow field around a deeply buried tunnel after excavation. Bull. Eng. Geol. Environ. 78 (1), 311–323.
Zheng, X., Yang, Z., Wang, S., Chen, Y.-F., Hu, R., Zhao, X.-J., Wu, X.-L., Yang, X.-L., 2020. Evaluation of hydrogeological impact of tunnel engineering in a karst aquifer by coupled discrete-continuum numerical simulations. J. Hydrol. 597, 125765.
Zheng, W., Wang, X.L., Tang, Y., Liu, H., Wang, M., Zhang, L.J., 2017. Use of tree rings as indicator for groundwater level drawdown caused by tunnel excavation in Zhongliang Mountains, Chongqing. Southwest China. Environ. Earth Sci. 76, 522.